International Journal of Pharmaceutics 630 (2023) 122422

Contents lists available at ScienceDirect

International Journal of Pharmaceutics

journal homepage: www.elsevier.com/locate/ijpharm

Magnesium stearate surface coverage on tablets and drug crystals: Insights from SEM-EDS elemental mapping

Chamara A. Gunawardana [a], Angela Kong [b], Daniel O. Blackwood [b], C. Travis Powell [b], Joseph F. Krzyzaniak [b], Myles C. Thomas [b], Changquan Calvin Sun [a,*]

[a] Pharmaceutical Materials Science and Engineering Laboratory, Department of Pharmaceutics, College of Pharmacy, University of Minnesota, Minneapolis, MN 55455, United States
[b] Pfizer Worldwide Research and Development, Groton, CT 06340, United States

ARTICLE INFO

Keywords:
scanning electron microscopy (SEM)
energy dispersive X-ray spectroscopy (EDS)
surface area coverage (SAC)
Elemental mapping
Chemical imaging
Magnesium stearate

ABSTRACT

Scanning electron microscopy-based energy dispersive X-ray spectroscopy (SEM-EDS) is proposed as a versatile tool for quantifying surface area coverage (SAC) by magnesium stearate (MgSt) on pharmaceutical tablets and particles. Our approach involved fast elemental mapping and subsequent SAC quantitation by image analysis. The study was conducted using a multi-component system, but the particle-level mapping was limited to active pharmaceutical ingredient (API) crystals. For both tablets and API particles, the calculated SAC against MgSt loading afforded a positive linear correlation over the range of MgSt levels examined in this work. On the tablet surface, MgSt was found to be preferentially concentrated at or in the close vicinity of grain boundaries, supporting the idea of compression-driven migration and relocation of MgSt within the tablet. On the particle surface, only discrete aggregates of MgSt were observed, as opposed to the widely accepted phenomenon of the formation of a thin lubricant film around host particles. The selection of proper SEM-EDS operating conditions and the challenges confronted in particle surface mapping are discussed in detail.

1. Introduction

Problems due to poor powder flowability, high tablet ejection force, abrasive tool wear, frictional heating, and punch sticking are commonplace in tablet manufacturing. Hence, lubricants are incorporated in tablet formulation to form an "internally lubricated" powder blend prior to compaction (Li and Wu, 2014; Miller and York, 1988; Morin and Briens, 2013; Strickland and Higuchi, 1960; Wang and Wen, 2010). The presence of a lubricant reduces inter-particulate and particle-tooling friction and adhesive interactions, which minimizes, if not eliminates, the above-mentioned issues.

While facilitating the manufacturing process, lubricants may also exert some negative impacts on the structural integrity and the performance of tablets. It is well known that magnesium stearate (MgSt), one of the most widely used solid lubricants in oral solid dosage forms, can reduce tablet mechanical strength and delay disintegration and dissolution (Strickland et al., 1956; Shotton and Lewis, 1964; Levy and Gumtow, 1963; Paul and Sun, 2018; Zuurman et al., 1999; Jarosz and Parrott, 1984). Moreover, the severity of those undesired effects depends markedly on both material properties and processing parameters, especially upon the degree of mixing (Kushner and Moore, 2010; Ganderton, 1969; Paul and Sun, 2017; Dun et al., 2020; Bolhuis et al., 1975; Lerk and Bolhuis, 1977; Lerk et al., 1977; Shah and Mlodozeniec, 1977; Johansson and Nicklasson, 1986; Lakio et al., 2013; Abe and Otsuka, 2012; Otsuka et al., 2004; Kikuta and Kitamori, 1994; Bolhuis et al., 1987; Ragnarsson et al., 1979; Bolhuis et al., 1981; Murthy and Samyn, 1977; De Boer et al., 1978). Hence, understanding the behavior of MgSt at the microstructural level is of paramount importance for effective development and optimization of formulations and drug product manufacturing processes.

Previous studies suggest that MgSt acts largely as a boundary lubricant, forming a hydrophobic, low-shear thin film around substrate particles that provides a sacrificial interfacial layer against rubbing/shear stresses (Bolhuis et al., 1975; Johansson and Nicklasson, 1986; Hussain et al., 1990; Hussain et al., 1988; Roblot-Treupel and Puisieux, 1986; Pintyehodi et al., 1981). During compression, however, an anisotropic re-distribution of MgSt from bulk to the periphery of the tablet can be expected, owing to its stress-induced deformation and

* Corresponding author at: 9-127B Weaver-Densford Hall, 308 Harvard Street S.E., Minneapolis, MN 55455, United States.
E-mail address: sunx0053@umn.edu (C. Calvin Sun).

https://doi.org/10.1016/j.ijpharm.2022.122422
Received 2 September 2022; Received in revised form 1 November 2022; Accepted 17 November 2022
Available online 19 November 2022

delamination, heat-induced melting/softening and subsequent flowing (Sun, 2015; Szalaya et al., 2004; Rubinstein and Moody, 1985). Therefore, in order to gain a more complete insight into the origin of its multifaceted functions, desired and undesired, it is important to study the distribution of MgSt at pre- and post-compression stages, that is, on both particle and tablet surface.

Scanning electron microscopy (SEM) is an invaluable tool for microstructure analysis of pharmaceutical systems, including tablets and powders (Klang et al., 2013). Thanks to its high resolving power, magnification range and focal depth, SEM can afford sharper images with fine structural details that are not visible with traditional optical microscopy. In SEM, the sample is irradiated with a finely focused, high-energy electron beam having a well-defined *de* Broglie wavelength. The interactions between this incident electron beam and atoms on the sample surface induce the emission of a number of different signals, carrying important information about the specimen. By scanning the electron beam/probe across the sample and by collecting a certain type of those signals, an image of the surface can be produced. For instance, secondary electrons (SEs), originated from the sample surface due to electron–electron inelastic scattering, can provide three-dimensional topographical contrast. Backscattered electrons (BSEs), that is, primary electrons elastically scattered by the atomic nuclei, can provide compositional contrast (*Z*-contrast) in the image where brighter regions correspond to high atomic number elements.

Inelastic scattering of primary beam electrons in SEM also induces the emission of X-rays from the sample, which serves as the basis for energy dispersive X-ray spectroscopy/spectrometry, commonly abbreviated as EDS or EDX (Goldstein et al., 2003). Incoming electrons collide with the electrons in low-lying orbitals of the atoms and eject them. Upper-level electrons then relax into those inner-shell vacancies, releasing the excess energy as X-ray photons. Since the energies of these emitted X-rays are characteristic of the material present, EDS effectively takes a fingerprint of the sample. By examining the intensity of the emissions, it is possible to determine how much of each element is present (Newbury and Ritchie, 2013). In EDS mapping, the electron probe moves over the surface in raster fashion, thereby compiling a map of surface composition (Friel and Lyman, 2006). Hence, when coupled to EDS, SEM can reveal the elements present, their concentrations and spatial distribution on the sample surface.

The initial applications of SEM-EDS in the field of pharmaceutical analysis can be traced back to the late 1970 s wherein the distribution of colloidal silica on sodium chloride particles was studied (Lerk and Bolhuis, 1977). Over the past few decades, its use has been continued in the field, either as a sole surface analytical method (Hussain et al., 1988; Roblot-Treupel and Puisieux, 1986; Pintyehodi et al., 1981; Steffens et al., 2020; Abreu-Villela et al., 2018; Sarecka-Hujar et al., 2017; Liu et al., 2009; McDermott et al., 2011; Nevsten et al., 2005; Ensslin et al., 2008; Seitavuopio et al., 2006) or in tandem with other related techniques (Gupta et al., 2022; Abreu-Villela et al., 2018; Katewongsa et al., 2017; Scoutaris et al., 2014; Vajna et al., 2011; Edge et al., 2002; Widjaja et al., 2011; Pajander et al., 2013), such as Raman chemical imaging (RCI) and time-of-flight secondary ion mass spectrometry (ToF-SIMS). Here we attempted to quantify the surface area coverage (SAC) by MgSt on tablets and active pharmaceutical ingredient (API) particles using SEM-EDS, which involved fast elemental mapping and subsequent image analysis.

2. Materials and methods

Ertugliflozin-pyroglutamic acid (1:1) co-crystal (ERT, Pfizer) was selected as a model drug (Duggirala et al., 2020). Excipients used in the study, microcrystalline cellulose (MCC; Avicel PH-102, DuPont), dicalcium phosphate anhydrate (DCPA; A-Tab, Innophos), crospovidone (Kollidon CL-SF, BASF) and magnesium stearate (MgSt; HyQual 5712, Mallinckrodt Pharmaceuticals), were all used as received.

2.1. Particle size analysis

The particle size distribution (PSD) of powders (Table 1) was measured using a laser diffraction particle size analyzer (HELOS, Sympatec Inc., Causthal-Zellerfeld, Germany).

2.2. Mixing and tableting

Eight different formulations were prepared with varying amounts of MgSt, from 0% to 4%, while keeping the API level constant at 40% (Table 2). Batch size was 5 g, and mixing was done in 20-mL containers (approximately 45 % headspace) at 49 rpm using a 3D shaker mixer (Turbula T2F, Willy A. Bachofen AG, Muttenz, Switzerland). First, ERT and all the excipients except MgSt were mixed for 30 min and, after adding MgSt, mixing was continued for 5 additional minutes.

Tablets were prepared using a compaction simulator (Styl'One Evolution, MedelPharm, Beynost, France) equipped with 8.00 mm, round flat-faced, TSM B-type tooling. A sample of ~ 100 mg was removed from each of the respective final blends and was manually filled into the die. A symmetrical, force-controlled, single compression cycle at 250 MPa was employed to compress the blend into a cylindrical tablet. The entire compression event consisted of a 1 s rise and a 1 s fall without holding at the maximum force, followed by 3 s relaxation, and a 2 s ejection step. Tablets were made following the order from F1 to F8, and the upper and lower punches and the die were thoroughly cleaned between formulations using isopropanol followed by acetone.

2.3. Scanning electron microscopy (SEM)

A field-emission SEM (JSM-6500F, JEOL ltd., Akishima, Tokyo, Japan) was used to collect images in the secondary electron image (SEI) mode. Samples were immobilized on aluminium stubs by means of double-sided carbon conductive tape and, prior to imaging, were coated with ca. 5 nm thick platinum using a high vacuum sputter coater (Leica EM ACE600, Leica Microsystems GmbH, Vienna, Austria).

2.4. Energy dispersive X-ray spectroscopy (EDS)

Samples for EDS mapping were mounted onto aluminium stubs using carbon conductive tape and coated with a thin layer of carbon using the Leica EM ACE600 coater via carbon thread evaporation. Mapping was performed on an Oxford Instruments microanalysis system consisting of an 80 mm^2 silicon drift detector (X-Max80, Oxford Instruments plc, Tubney Woods, Abingdon, UK) attached to the JEOL JSM-6500F FE-SEM. Its in-built AZtec 4.2 software (Oxford Instruments Nanotechnology Tools Limited, Tubney Woods, Abingdon, Oxon, UK) was used for image capturing and preliminary processing.

Tablet samples were coated with ca. 5 nm thick carbon film before mapping. For each tablet, three randomly chosen sites on the surface were mapped using the following settings: acceleration voltage of 10 kV, probe current of 16 (corresponding to ca. 8nA), working distance of 10 ± 1 mm, magnification of × 500 (corresponding to a field of view, FOV, of 254 μm × 190.4 μm), resolution of 2048 × 1536, frame count of 3, process time of 4, and pixel dwell time of 20 μs.

Samples of final blends for EDS mapping were coated with ca. 10 nm thick carbon before being analyzed. Imaging was performed with the

Table 1
Particle size distribution data of materials used in this work.

Material	D10 (μm)	D50 (μm)	D90 (μm)	D[4,3] (μm)
ERT	7	43	111	52
MCC	31	108	234	122
DCPA	50	191	301	184
Crospovidone	6	20	54	26
MgSt	1.8	6.1	12.8	6.8

Table 2
Components and composition of the different formulations prepared.

Ingredient	Amount (%)							
	F1	F2	F3	F4	F5	F6	F7	F8
ERT	40.00	40.00	40.00	40.00	40.00	40.00	40.00	40.00
MCC	30.00	30.00	30.00	30.00	30.00	30.00	30.00	30.00
DCPA	27.00	26.85	26.70	26.50	26.00	25.00	24.00	23.00
Crospovidone	3.00	3.00	3.00	3.00	3.00	3.00	3.00	3.00
MgSt	0.00	0.15	0.30	0.50	1.00	2.00	3.00	4.00

following system parameters: acceleration voltage of 10 kV, probe current of 13 (corresponding to ca. 0.6 nA), working distance of 10 ± 1 mm, magnification of × 2000 (corresponding to a FOV of 63.5 μm × 47.6 μm), resolution of 1024 × 768 pixels, frame count of 2, process time of 6, and pixel dwell time of 50 μs.

2.5. Image analysis

All captured magnesium (Mg) maps were saved in TIFF format without any annotations, while preserving the original resolution and aspect ratio. Further processing (sharpening the boundaries of Mg-containing domains and removing the background noise) and the quantification of SAC was done with Fiji software (Schindelin et al., 2012). For the SAC quantification on tablet surface, each original Mg map was smoothed by applying the "Gaussian Blur…" filter with a standard deviation (σ) of 4.00 pixels and then converted into grayscale (8-bit). After auto-thresholding with the "Yen" method in black background, the area fractions were directly obtained. Particle surface images were treated in the same manner except that a σ radius of 6.00 was used in the blurring step. Detailed workflow can be found in SI.

3. Results and discussion

3.1. Optimizing EDS mapping parameters

When performing SEM-EDS analysis, one needs to consider the operating conditions of both SEM and EDS, which are often interrelated in a rather complicated manner. Hence, they need to be carefully optimized, on a case-by-case basis, according to the nature of the sample being analyzed and the level of information needed. One of the key parameters is the beam energy, or the accelerating voltage. In SEM, higher accelerating voltage results in smaller probe size and, hence, higher spatial resolution. However, it can also lead to reduced image contrast, disappearance of fine structural features, and more interference from the bulk of the sample for surface imaging and mapping, because of the diffusion of the beam over a large volume.

A lower accelerating voltage is preferred in EDS analysis because of some key benefits, namely enhanced spatial resolution, sensitivity, and surface selectivity, all linked to the reduced spread of electron beam within the sample (Wuhrer and Moran, 2016). Low-kV EDS also lessens the risk of charge build-up, heating and sample damage. For particle-level analysis, it helps to reduce the mass and absorption effects and, hence, the associated uncertainties (Small, 2002). The electron beam should, however, have sufficient energy to overcome the electron binding energies and to allow atomic transitions that produce characteristic X-rays from all the elements of interest. It is common practice to keep the overvoltage (i.e., the ratio between the beam energy and the critical excitation energy/ionization potential of the analytes) somewhere around two to three. Considering all these facts, an accelerating voltage of 10 kV was used throughout this study for EDS mapping on tablets and particles.

The system dead time, expressed as a percentage of real time (i.e., *100(ICR–OCR)/ICR*, where *ICR* and *OCR* are input and output count rates, respectively), should also be maintained within an appropriate or recommended range. It is a measure of the length of time when the EDS pulse processor is occupied processing the X-ray signals (or rejecting them in case of pulse pile-up) and is not available for incoming X-rays. Dead time can be controlled primarily by adjusting the probe current and/or the process time. Increase in probe current increases the signal-to-noise ratio (SNR) but deteriorated spatial resolution (due to larger spot size), sample charging, and beam damage would be concerns. In EDS, higher probe current is particularly useful to increase the X-ray throughput (high ICR) and, hence, the dead time. The process time (or the time constant) is a measure of the length of time the EDS pulse processor spent in measuring the incoming X-ray signals and in reducing the noise. A longer process time decreases the OCR, thereby increasing the dead time. It also increases the energy resolution but at the expense of the throughput, that is, the actual time required for the analysis. In our study, the probe current and the process time were adjusted so as to obtain a dead time of 35–40% during mapping. An ICR of around 65,000 counts per second (cps) and an OCR of around 40,000 cps were observed for the tablet samples, whereas those for the ERT particles were around 15,000 cps and 9000 cps, respectively.

When mapping, the electron beam dwells on each pixel for a specified length of time while collecting X-rays and then moves to the next one. In order to further reduce the temporary sample strain from the electron bombardment and potential radiation damage, frame averaging with shorter dwell time per pixel (i.e., several fast scans) was employed. For every image, three cycles of acquisition per image were taken by using 20 μs dwell time. The working distance was kept constant at 10 mm because the system, including the X-ray detector, sample chamber, etc., was configured to achieve the optimum detection efficiency at that value. With the final set of system parameters used (see Section 2.4), the total acquisition time per image for tablet and particle samples were around 5.5 and 3.5 min, respectively.

3.2. Tablet surface mapping

ERT, DCPA and MgSt are readily identifiable from the mapping images (Fig. 1) since they all have unique element(s) with non-overlapping peaks. The main analyte, MgSt ($Mg(C_{18}H_{35}O_2)_2$), gives a distinctive peak at 1.253 keV for magnesium. Chorine in ERT ($C_{22}H_{25}ClO_7{\cdot}C_5H_7NO_3$) and, calcium and phosphorous in DCPA ($CaHPO_4$) show up at 2.621, 3.690 and 2.013 keV, respectively. However, MCC ($(C_6H_{10}O_5)_n$) and crospovidone ($(C_6H_9NO)_n$), are not distinguishable unambiguously from EDS mapping. Consistent with the 40% w/w loading, ERT grains occupy approximately half of the image area. Even though the original ERT particles are highly deformed after compaction, their cross-sectional shape is mostly retained. Interestingly, MgSt seemed to reside mostly at or near the grain boundaries, supporting the common belief of compression-driven migration and relocation of MgSt within the tablet (Sun, 2015; Rubinstein and Moody, 1985).

Fig. 2 shows a collection of Mg maps obtained for tablets with different MgSt contents. As expected, SAC on tablet surface by Mg gradually increases with the MgSt concentration (from left to right). However, all maps comprised a significant amount of background noise that could interfere with the image analysis based SAC quantification. A number of de-noisification methods were assessed, by using the images of the tablet with 0% MgSt as a guide (negative control). The protocol

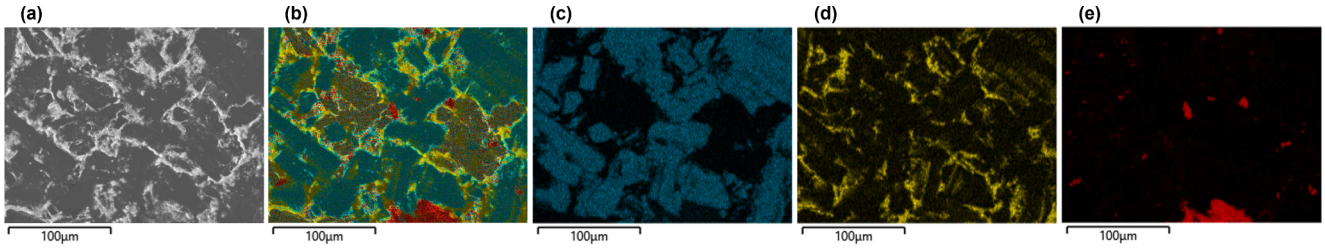

Fig. 1. A representative set of EDS images obtained for a single site on a tablet surface (×500, image area = 254 μm × 190.4 μm, see Figure S1 for the complete series). (a) electron image, (b) composite image, (c) chlorine map, (d) magnesium map, and (e) calcium map. Phosphorous map, which is virtually identical to the calcium map, is omitted for clarity.

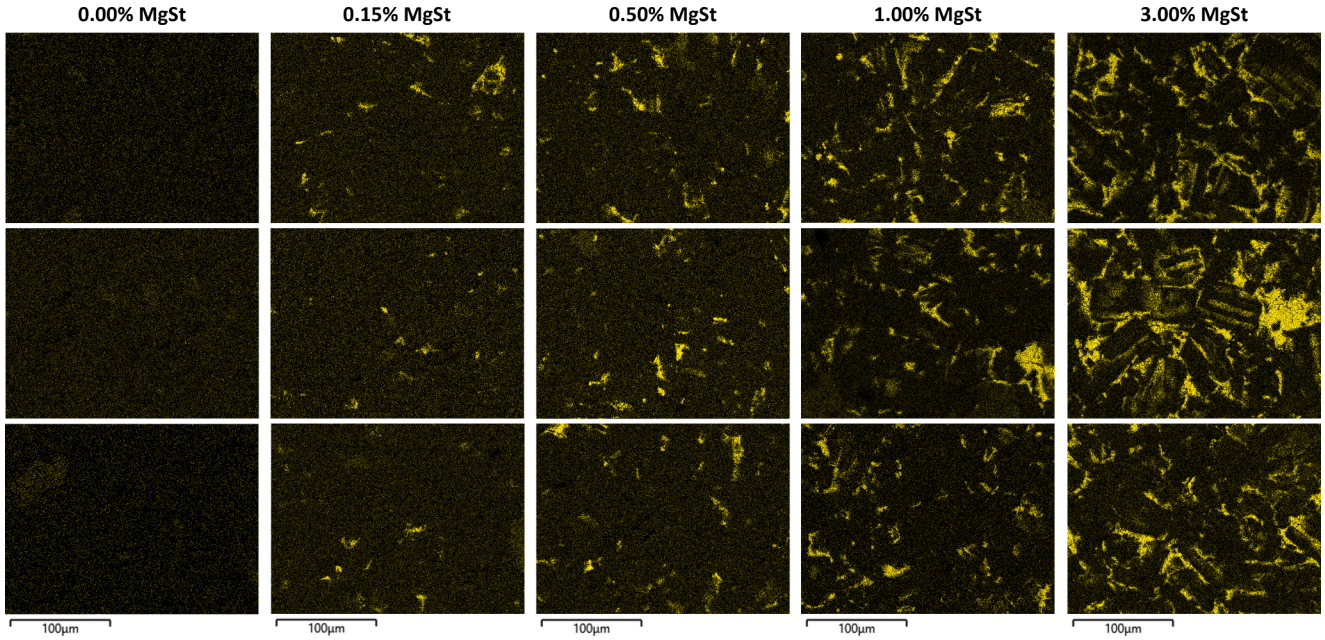

Fig. 2. EDS Mg maps of the tablet surface for five selected MgSt levels (×500, image area = 254 μm × 190.4 μm, see Figure S2 for the complete series). The three images in each column represents the three sites mapped on the tablet surface. All images have been binned (binning factor = 4) to improve the contrast and brightness.

outlined in Section 2.5 offered the best results with near-zero SAC for the tablet containing no MgSt. The same mapping and post-processing parameters along with a predetermined image size throughout helped to avoid any subjective artifacts, which may occur, for example, when defining regions of interest (ROIs) manually. The SAC calculated in this manner correlates linearly with the MgSt concentration (Fig. 3a), even though there are relatively large standard deviations.

3.3. Particle surface mapping

Mapping and subsequent quantification of SAC at particle level was quite challenging due to a series of factors. First, all types of particles in our formulation have a variety of sizes and shapes, and their surfaces are quite rough (Fig. 4). EDS, like many other surface imaging and mapping techniques, requires the sample surface be flat and smooth. In fact,

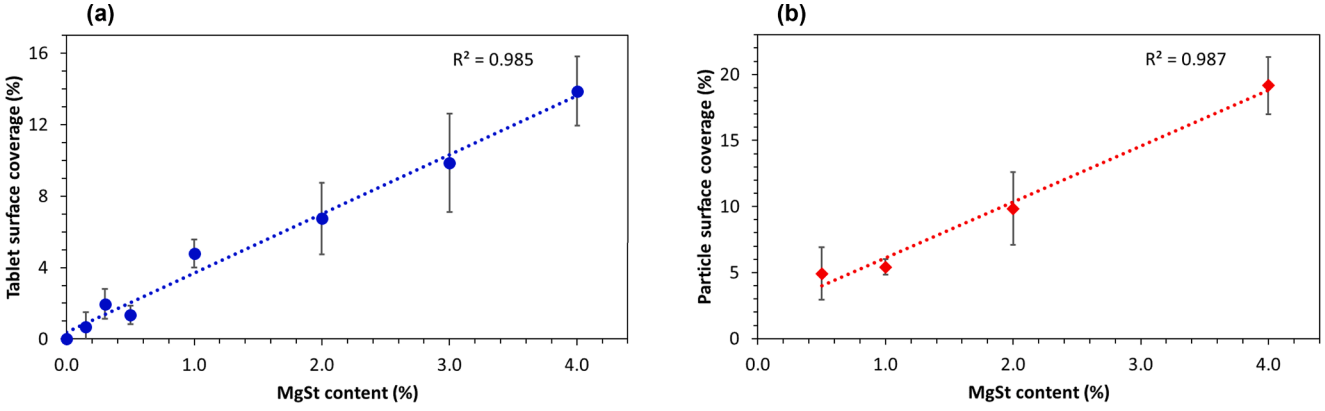

Fig. 3. Relationship between surface coverage and MgSt loading for (a) tablets and (b) ERT particles. Error bars indicate the standard deviation (n = 3).

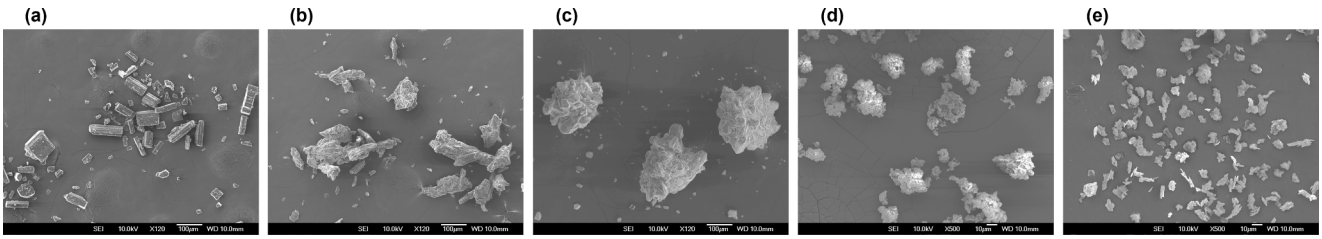

Fig. 4. SEM images of formulation ingredients. (a) ERT (×120), (b) MCC (×120), (c) DCPA (×120), (d) crospovidone (×500), and (e) MgSt (×500).

performing EDS analysis on a coarse, uneven surface creates its own inherent artifacts, namely shadowing and topographic effects. Shadowing arises from the partial or complete blockage of X-rays from reaching the detector by adjacent surface asperities and/or neighboring particles. Complex topography causes fluctuation of incident and take-off angles from one point to another, which in turn influences the characteristic peak intensities. Secondly, unlike tablet samples, all particles exhibited a relatively high susceptibility to charge build-up and beam damage, which is likely promoted by surface asperities.

Since ERT particles assumed a columnar (rectangular rod-like) habit, a reasonably flat surface was able to be brought to the field of view at higher magnifications (×2000 or higher), by choosing larger ERT crystals. Even though the surfaces still contained fine crystals, terraces, ledges and grooves, it was deemed effort-worthy to analyze at least a selected set of powder samples via EDS mapping. To avoid the shadowing effects by neighboring particles, care was taken to sprinkle the powder on the adhesive tape as lightly as possible when preparing samples of final blends for mapping. Rather fast surface degradation was the next issue, where MgSt particles underwent easy deformation, and occasional detaching and drifting with prolonged exposure. Therefore, the carbon coating thickness was doubled and the probe current for mapping was reduced. To bring the dead time back to an acceptable range, process time was increased to its maximum. All these led to relatively low X-ray count rates and, to compensate for that, the dwell time was slightly increased.

Only ERT crystals meeting certain quality criteria were mapped, and consequently sampling bias was inevitable. Moreover, each EDS map covered only a small area per image (63.5 μm × 47.6 μm) on the particle surface. Hence, results may not be representative of the bulk powder. Nevertheless, as for the tablet surface, a linear relationship between the level of MgSt used in formulations and percent area of ERT crystals covered by MgSt was found (Fig. 3b). Most importantly, particle level EDS mapping was able to offer new insights into the distribution of MgSt on particle surface. In contrast to previous studies that claim the formation of a thin, continuous MgSt coating around host particles (Bolhuis et al., 1975; Johansson and Nicklasson, 1986; Hussain et al., 1990; Hussain et al., 1988; Roblot-Treupel and Puisieux, 1986; Pintyehodi et al., 1981), here MgSt exists on ERT particles only as isolated units (Fig. 5), with no noticeable changes in original particle size or their rosette- or crumpled paper-like appearance. Since the formation of a thin lubricant film requires shearing off (or delamination) of MgSt particles during the mixing process (Ertel and Carstensen, 1988; Wada and Matsubara, 1994), its absence suggests that these events have not occurred under the mixing conditions used in this study. Factors that can affect the delamination and distribution of MgSt during mixing include batch size, headspace, and mixing time and intensity. Another

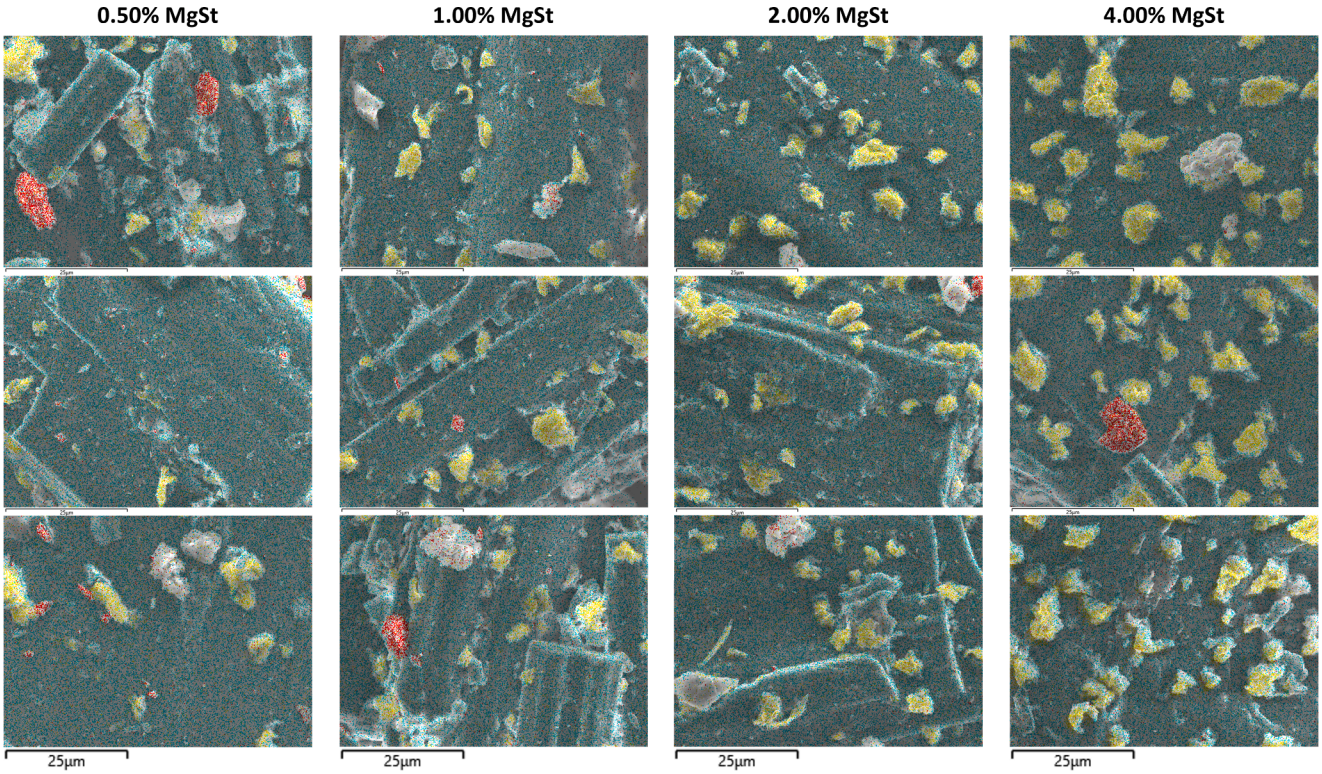

Fig. 5. Particle surface composite maps (×2000, image area = 63.5 μm × 47.6 μm, see Figure S3 for the corresponding Mg maps). The three images in each column represents three separate ERT particles chosen from the same final blend. Color coding: ERT (cyan), MgSt (yellow), DCPA (red).

possibility is the presence of an ultra-thin MgSt film (in addition to the discrete aggregates observed), with only a few molecular layers of thickness, which is below the limit of detection of EDS (Zhou et al., 2011).

3.4. Important considerations regarding EDS analysis

Here EDS was used in its standardless, semi-quantitative mode, in which the peak intensities are normalized to 100% based on the elements detected to determine their relative abundance. Our main objective was to quantify the area fraction or percentage covered by MgSt, rather than to determine the actual amount of MgSt present on the tablet or particle surface. Once the EDS elemental maps were collected, surface coverage was quantified separately by image analysis. It should be noted that the SAC calculations directly depend on the acquisition, processing and analysis parameters used. Hence, in order to produce unbiased and reproducible quantitative results and to enable reliable comparison among images, one needs to adhere to the same set of parameters throughout. For the same reasons, it is crucial to report all relevant image analysis steps and parameters along with the results (Figures S4–S7).

Not every inelastic scattering event leads to electronic excitation or ionization. Due to the electric field surrounding the nuclei of the atoms in the sample, the primary-beam electrons can decelerate, deflect and lose energy. Some of this energy is converted to X-rays with a range of energies/wavelengths, called bremsstrahlung or braking radiation (also commonly referred to as non-characteristic, polychromatic, continuous, white or background radiation). Hence, irrespective of the presence or absence of random noise, EDS spectra inherently consist of a broad, featureless bremsstrahlung noise, with high-intensity, sharp characteristic peaks from samples superimposed on it. Because of the bremsstrahlung background, the identification of low-intensity characteristic X-ray peaks may become very difficult, which limits the sensitivity of EDS analysis.

As mentioned earlier in Section 3.3, flat and polished sample surface remains a key prerequisite for eliminating the shadowing and topographic effects for reliable EDS results. Experimental modifications, such as collecting a set of mapping images with sample/stage rotation and subsequent merging, or instrument modifications, such as multi-detector configurations, can lessen this effect when analyzing rough surfaces.

It is also important to remember that EDS is not strictly a surface technique as the electron beam may penetrate further into the sample, generating X-rays from deeper subsurface regions. The penetration depth can be controlled to some extent by reducing the beam energy and/or by tilting the sample with respect to the electron probe. Overall, EDS is less surface selective than other related techniques, such as X-ray photoelectron spectroscopy (XPS) and scanning Auger microscopy (SAM). These latter techniques, however, have their own drawbacks. For example, XPS generally suffers from limited spatial resolution and high time-consumption.

Apart from the disadvantages and complications highlighted above, modern SEM-EDS systems are capable of detecting elements from lithium and upwards. Thanks to silicon drift detectors (SDDs) with increased active areas, they have excellent energy resolution at high count rates, much improved signal collection efficiencies and, hence, better SNRs (Newbury and Ritchie, 2013). Windowless SDD detectors can deliver greater sensitivity towards light elements, especially from lithium to neon. The associated software offers advanced algorithms for peak deconvolution, background subtraction, and for correcting pulse pile-up, sample drift and matrix effects. Other valuable features include real-time chemical imaging and large area mapping capabilities. With all these advances, SEM-EDS possesses the ability to deliver fast and reliable results to be a powerful tool in characterizing pharmaceutical materials. It can certainly supplement and complement other commonly used chemical imaging and mapping techniques, such as Raman, near-infrared (NIR), and time-of-flight secondary ion mass spectrometry (ToF-SIMS).

Finally, the approach that we have shown here can easily be extended to formulations containing other lubricants, such as sodium stearyl fumarate (SSF), hydrated magnesium silicate (talc), amorphous silicon dioxide (fumed silica), provided they contain no additional sources of respective element(s) of interest. The knowledge derived from an EDS-based method can then be used to elucidate the effect of a particular lubricant on pharmaceutically important properties, such as tablet ejection force, tensile strength, and dissolution rate. In this context, our current efforts are focused on exploring the impact of MgSt distribution on punch sticking propensity of sticky APIs. Mechanistic understanding from that work is expected to guide formulation design and process optimization to mitigate possible punch sticking problems during tablet manufacturing.

4. Conclusions

Scanning electron microscopy combined with energy dispersive X-ray spectroscopy (SEM-EDS) offers element specific mapping of a surface at the micro length scale. Such information can provide valuable insights into the bulk properties during pharmaceutical processing. Using ertugliflozin-pyroglutamic acid co-crystal as a model drug, we have demonstrated that EDS-based elemental mapping can be used to visualize, map, and quantify the common lubricant, magnesium stearate (MgSt), on multi-component tablets as well as on the surface of drug particles. Tablet surface analysis showed that MgSt occupies mostly at or near the grain boundaries, suggesting the occurrence of MgSt migration and relocation events during compression. Moreover, particle level mapping revealed that MgSt exists on the surface of ERT crystals only as isolated units, with no signs of the presence of a continuous lubricant film.

CRediT authorship contribution statement

Chamara A. Gunawardana: Data curation, Formal analysis, Writing – original draft, Writing – review & editing. **Angela Kong:** Project administration, Formal analysis, Writing – review & editing. **Daniel O. Blackwood:** Formal analysis, Writing – review & editing. **C. Travis Powell:** Formal analysis, Writing – review & editing. **Joseph F. Krzyzaniak:** Formal analysis, Writing – review & editing. **Myles Thomas:** Formal analysis, Writing – review & editing. **Changquan Calvin Sun:** Funding acquisition, Supervision, Conceptualization, Supervision, Project administration, Writing – review & editing.

Declaration of Competing Interest

The authors declare that they have no known competing financial interests or personal relationships that could have appeared to influence the work reported in this paper.

Data availability

Data will be made available on request.

Acknowledgements

This work was supported by a grant from Pfizer Inc. Parts of this work were carried out in the Characterization Facility, University of Minnesota, which receives partial support from the NSF through the MRSEC (Award Number DMR-2011401) and the NNCI (Award Number ECCS-2025124) programs.

Appendix A. Supplementary material

Supplementary data to this article can be found online at https://doi.

org/10.1016/j.ijpharm.2022.122422.

References

Abe, H., Otsuska, M., 2012. Effects of lubricant-mixing time on prolongation of dissolution time and its prediction by measuring near infrared spectra from tablets. Drug Dev. Ind. Pharm. 38, 412–419.

Abreu-Villela, R., Adler, C., Caraballo, I., Kuentz, M., 2018. Electron microscopy/energy dispersive X-ray spectroscopy of drug distribution in solid dispersions and interpretation by multifractal geometry. J. Pharm. Biomed. Anal. 150, 241–247.

Abreu-Villela, R., Schönenberger, M., Caraballo, I., Kuentz, M., 2018. Early stages of drug crystallization from amorphous solid dispersion via fractal analysis based on chemical imaging. Eur. J. Pharm. Biopharm. 133, 122–130.

Bolhuis, G., Lerk, C., Zijlstra, H., De Boer, A., 1975. Film formation by magnesium stearate during mixing and its effect on tabletting. Pharm. Weekbl. 110, 317–325.

Bolhuis, G.K., De Jong, S.W., Lerk, C.F., Dettmers, H., Pharbita, B.V., 1987. The effect of magnesium stearate admixing in different types of laboratory and industrial mixers on tablet crushing strength. Drug Dev. Ind. Pharm. 13, 1547–1567.

Bolhuis, G.K., Smallenbroek, A.J., Lerk, C.F., 1981. Interaction of tablet disintegrants and magnesium stearate during mixing I: effect on tablet disintegration. J. Pharm. Sci. 70, 1328–1330.

De Boer, A.H., Bolhuis, G.K., Lerk, C.F., 1978. Bonding characteristics by scanning electron microscopy of powders mixed with magnesium stearate. Powder Technol. 20, 75–82.

Duggirala, N.K., LaCasse, S.M., Zaworotko, M.J., Krzyzaniak, J.F., Arora, K.K., 2020. Pharmaceutical cocrystals: formulation approaches to develop robust drug products. Cryst. Growth Des. 20, 617–626.

Dun, J., Chen, H., Sun, C.C., 2020. Profound tabletability deterioration of microcrystalline cellulose by magnesium stearate. Int. J. Pharm. 590, 119927.

Edge, S., Belu, A.M., Potter, U.J., Steele, D.F., Young, P.M., Price, R., Staniforth, J.N., 2002. Chemical characterisation of sodium starch glycolate particles. Int. J. Pharm. 240, 67–78.

Ensslin, S., Moll, K.P., Paulus, K., Mäder, K., 2008. New insight into modified release pellets – Internal structure and drug release mechanism. J. Controlled Release 128, 149–156.

Ertel, K.D., Carstensen, J.T., 1988. Chemical, Physical, and Lubricant Properties of Magnesium Stearate. J. Pharm. Sci. 77, 625–629.

Friel, J.J., Lyman, C.E., 2006. Tutorial Review: X-ray Mapping in Electron-Beam Instruments. Microsc. Microanal. 12, 2–25.

Ganderton, D., 1969. The effect of distribution of magnesium stearate on the penetration of a tablet by water. J. Pharm. Pharmacol. 21, 9S–18S.

Goldstein, J.I., Newbury, D.E., Echlin, P., Joy, D.C., Lyman, C.E., Lifshin, E., Sawyer, L., Michael, J.R., 2003. Scanning Electron Microscopy and X-ray Microanalysis, Third ed. Springer, Boston, MA.

Gupta, S., Omar, T., Muzzio, F.J., 2022. SEM/EDX and Raman chemical imaging of pharmaceutical tablets: a comparison of tablet surface preparation and analysis methods. Int. J. Pharm. 611, 121331.

Hussain, M.S.H., York, P., Timmins, P., 1988. A study of the formation of magnesium stearate film on sodium chloride using energy-dispersive X-ray analysis. Int. J. Pharm. 42, 89–95.

Hussain, M.S.H., York, P., Timmins, P., Humphrey, P., 1990. Secondary ion mass spectrometry (SIMS) evaluation of magnesium stearate distribution and its effects on the physico-technical properties of sodium chloride tablets. Powder Technol. 60, 39–45.

Jarosz, P.J., Parrott, E.L., 1984. Effect of Lubricants on Tensile Strengths of Tablets. Drug Dev. Ind. Pharm. 10, 259–273.

Johansson, M.E., Nicklasson, M., 1986. Investigation of the film formation of magnesium stearate by applying a flow-through dissolution technique. J. Pharm. Pharmacol. 38, 51–54.

Katewongsa, P., Terada, K., Phaechamud, T., 2017. Spatial distributing lubricants from Raman mapping and scanning electron microscopy–energy dispersive X-ray spectroscopy on cetirizine dihydrochloride fast disintegrating tablet properties. J. Pharm. Investig. 47, 249–262.

Kikuta, J.-I., Kitamori, N., 1994. Effect of Mixing Time on the Lubricating Properties of Magnesium Stearate and the Final Characteristics of the Compressed Tablets. Drug Dev. Ind. Pharm. 20, 343–355.

Klang, V., Valenta, C., Matsko, N.B., 2013. Electron microscopy of pharmaceutical systems. Micron 44, 45–74.

Kushner, J., Moore, F., 2010. Scale-up model describing the impact of lubrication on tablet tensile strength. Int. J. Pharm. 399, 19–30.

Lakio, S., Vajna, B., Farkas, I., Salokangas, H., Marosi, G., Yliruusi, J., 2013. Challenges in Detecting Magnesium Stearate Distribution in Tablets. AAPS PharmSciTech 14, 435–444.

Lerk, C.F., Bolhuis, G.K., 1977. Interaction of lubricants and colloidal silica during mixing with excipients. II. Its effect on wettability and dissolution velocity. Pharm. Acta Helv. 52, 39–44.

Lerk, C.F., Bolhuis, G.K., Smedema, S.S., 1977. Interaction of lubricants and colloidal silica during mixing with excipients. I. Its effect on tabletting. Pharm. Acta Helv. 52, 33–39.

Levy, G., Gumtow, R.H., 1963. Effect of Certain Tablet Formulation Factors on Dissolution Rate of the Active Ingredient III. J. Pharm. Sci. 52, 1139–1144.

Li, J., Wu, Y., 2014. Lubricants in Pharmaceutical Solid Dosage Forms. Lubricants 2, 21–43.

Liu, F., Lizio, R., Schneider, U.J., Petereit, H.-U., Blakey, P., Basit, A.W., 2009. SEM/EDX and confocal microscopy analysis of novel and conventional enteric-coated systems. Int. J. Pharm. 369, 72–78.

McDermott, T.S., Farrenkopf, J., Hlinak, A., Neilly, J.P., Sauer, D., 2011. A material sparing method for quantitatively measuring tablet sticking. Powder Technol. 212, 240–252.

Miller, T.A., York, P., 1988. Pharmaceutical tablet lubrication. Int. J. Pharm. 41, 1–19.

Morin, G., Briens, L., 2013. The Effect of Lubricants on Powder Flowability for Pharmaceutical Application. AAPS PharmSciTech 14, 1158–1168.

Murthy, K.S., Samyn, J.C., 1977. Effect of shear mixing on in vitro drug release of capsule formulations containing lubricants. J. Pharm. Sci. 66, 1215–1219.

Nevsten, P., Borgquist, P., Axelsson, A., Wallenberg, L.R., 2005. XEDS-mapping for explaining release patterns from single pellets. Int. J. Pharm. 290, 109–120.

Newbury, D.E., Ritchie, N.W.M., 2013. Elemental mapping of microstructures by scanning electron microscopy-energy dispersive X-ray spectrometry (SEM-EDS): extraordinary advances with the silicon drift detector (SDD). J. Anal. At. Spectrom. 28, 973–988.

Newbury, D.E., Ritchie, N.W.M., 2013. Is Scanning Electron Microscopy/Energy Dispersive X-ray Spectrometry (SEM/EDS) Quantitative? Scanning 35, 141–168.

Otsuka, M., Yamane, I., Matsuda, Y., 2004. Effects of lubricant mixing on compression properties of various kinds of direct compression excipients and physical properties of the tablets. Adv. Powder Technol. 15, 477–493.

Pajander, J., Haugshøj, K.B., Bjørneboe, K., Wahlberg, P., Rantanen, J., 2013. Foreign matter identification from solid dosage forms. J. Pharm. Biomed. Anal. 80, 116–125.

Paul, S., Sun, C.C., 2017. Lubrication with magnesium stearate increases tablet brittleness. Powder Technol. 309, 126–132.

Paul, S., Sun, C.C., 2018. Systematic evaluation of common lubricants for optimal use in tablet formulation. Eur. J. Pharm. Sci. 117, 118–127.

Pintyehodi, K., Toth, I., Kata, M., 1981. Investigation of the formation of magnesium stearate film by energy dispersive-X-ray microanalysis. Pharm. Acta Helv. 56, 320–324.

Ragnarsson, G., Hölzer, A.W., Sjögren, J., 1979. The influence of mixing time and colloidal silica on the lubricating properties of magnesium stearate. Int. J. Pharm. 3, 127–131.

Roblot-Treupel, L., Puisieux, F., 1986. Distribution of magnesium stearate on the surface of lubricated particles. Int. J. Pharm. 31, 131–136.

M, Rubinstein, G, Moody, 1985. Migration of magnesium stearate during tablet production. Expo-Congr. lnt. Technol. Pharm 3rd, 5, 7-11, Association de Pharmacie Galenique Industrielle.

Sarecka-Hujar, B., Balwierz, R., Ostrozka-Cieslik, A., Dyja, R., Lukowiec, D., Jankowski, A., 2017. Scanning electron microscopy and X-ray energy dispersive spectroscopy – useful tools in the analysis of pharmaceutical products. J. Phys. Conf. Ser. 931, 012008.

Schindelin, J., Arganda-Carreras, I., Frise, E., Kaynig, V., Longair, M., Pietzsch, T., Preibisch, S., Rueden, C., Saalfeld, S., Schmid, B., Tinevez, J.-Y., White, D.J., Hartenstein, V., Eliceiri, K., Tomancak, P., Cardona, A., 2012. Fiji: an open-source platform for biological-image analysis. Nat. Methods 9, 676–682.

Scoutaris, N., Vithani, K., Slipper, I., Chowdhry, B., Douroumis, D., 2014. SEM/EDX and confocal Raman microscopy as complementary tools for the characterization of pharmaceutical tablets. Int. J. Pharm. 470, 88–98.

Seitavuopio, P., Heinämäki, J., Rantanen, J., Yliruusi, J., 2006. Monitoring tablet surface roughness during the film coating process. AAPS PharmSciTech 7, E1–E6.

Shah, A.C., Mlodozeniec, A.R., 1977. Mechanism of Surface Lubrication: influence of duration of lubricant-excipient mixing on processing characteristics of powders properties of compressed tablets. J. Pharm. Sci. 66, 1377–1382.

Shotton, E., Lewis, C.J., 1964. Some observations on the effect of lubrication on the crushing strength of tablets. J. Pharm. Pharmacol. 16, 111T–120T.

Small, J.A., 2002. The Analysis of Particles at Low Accelerating Voltages (≤ 10 kV) With Energy Dispersive X-Ray Spectroscopy (EDS). J. Res. Natl. Inst. Stand. Technol. 107, 555–566.

Steffens, K.E., Brenner, M.B., Hartig, M.U., Monschke, M., Wagner, K.G., 2020. Melt granulation: A comparison of granules produced via high-shear mixing and twin-screw granulation. Int. J. Pharm. 591, 119941.

Strickland Jr, W.A., Nelson, E., Busse, L.W., Higuchi, T., 1956. The physics of tablet compression IX. Fundamental aspects of tablet lubrication. J. Am. Pharm. Assoc. 45, 51–55.

Strickland, W.A., Higuchi, T., Busse, L.W., 1960. The Physics of Tablet Compression X**Received June 25, 1959, from the School of Pharmacy, University of Arkansas, Little Rock.: Mechanism of Action and Evaluation of Tablet Lubricants. J. Am. Pharmaceutical Association (Scientific ed.) 49, 35–40.

Sun, C.C., 2015. Dependence of ejection force on tableting speed—a compaction simulation study. Powder Technol. 279, 123–126.

Szalaya, A., Pintye-Hodi, K., Joo, K., Erös, I., 2004. Study of the distribution of magnesium stearate with an energy dispersive X-ray fluorescence analyser. Pharmazeutische. Industrie. 66, 221–223.

Vajna, B., Farkas, I., Farkas, A., Pataki, H., Nagy, Z., Madarász, J., Marosi, G., 2011. Characterization of drug–cyclodextrin formulations using Raman mapping and multivariate curve resolution. J. Pharm. Biomed. Anal. 56, 38–44.

Wada, Y., Matsubara, T., 1994. Pseudopolymorphism and lubricating properties of magnesium stearate. Powder Technol. 78, 109–114.

Wang, J., Wen, H., Desai, D., 2010. Lubrication in tablet formulations. Eur. J. Pharm. Biopharm. 75, 1–15.

Widjaja, E., Kanaujia, P., Lau, G., Ng, W.K., Garland, M., Saal, C., Hanefeld, A., Fischbach, M., Maio, M., Tan, R.B.H., 2011. Detection of trace crystallinity in an amorphous system using Raman microscopy and chemometric analysis. Eur. J. Pharm. Sci. 42, 45–54.

Wuhrer, R., Moran, K., 2016. Low voltage imaging and X-ray microanalysis in the SEM: challenges and opportunities. IOP Conference Series: Mater. Sci. Eng. 109, 012019.
Zhou, Q., Denman, J.A., Gengenbach, T., Das, S., Qu, L., Zhang, H., Larson, I., Stewart, P. J., Morton, D.A.V., 2011. Characterization of the surface properties of a model pharmaceutical fine powder modified with a pharmaceutical lubricant to improve flow via a mechanical dry coating approach. J. Pharm. Sci. 100, 3421–3430.
Zuurman, K., Van der Voort Maarschalk, K., Bolhuis, G.K., 1999. Effect of magnesium stearate on bonding and porosity expansion of tablets produced from materials with different consolidation properties. Int. J. Pharm. 179, 107–115.